Statistics and Computing
https://doi.org/10.1007/s11222-020-09956-4

# Simulating space-time random fields with nonseparable Gneiting-type covariance functions

**Denis Allard**[1] · **Xavier Emery**[2,3] · **Céline Lacaux**[4] · **Christian Lantuéjoul**[5]

Received: 8 November 2019 / Accepted: 3 June 2020


**Abstract**
Two algorithms are proposed to simulate space-time Gaussian random fields with a covariance function belonging to an extended Gneiting class, the definition of which depends on a completely monotone function associated with the spatial structure and a conditionally negative definite function associated with the temporal structure. In both cases, the simulated random field is constructed as a weighted sum of cosine waves, with a Gaussian spatial frequency vector and a uniform phase. The difference lies in the way to handle the temporal component. The first algorithm relies on a spectral decomposition in order to simulate a temporal frequency conditional upon the spatial one, while in the second algorithm the temporal frequency is replaced by an intrinsic random field whose variogram is proportional to the conditionally negative definite function associated with the temporal structure. Both algorithms are scalable as their computational cost is proportional to the number of space-time locations that may be irregular in space and time. They are illustrated and validated through synthetic examples.

**Keywords** Spectral simulation · Spectral measure · Substitution random field · Gaussian random field

## 1 Introduction

The simulation of random fields plays an increasingly important role in environmental and climate studies, for example to quantify uncertainties and to assess adaptation scenarios to global changes. Space-time simulations that span over relatively large regions and long periods of time generate very large space-time grids as soon as the resolution is not coarse. However, simulating space-time random fields on very large grids remains a challenge, in particular for nonseparable covariance functions able to capture space-time complexity, such as the Gneiting class of covariance functions (Gneiting 2002). This motivation prompted this research.

In the following, $Z(\boldsymbol{x}, t)$ will denote a space-time random field defined over $\mathbb{R}^k \times \mathbb{R}$, where $k$ is the space dimension, with $k = 2$ or $k = 3$ in most applications. Here, and in the rest of this work, we will use roman letters for scalars and bold letters for vectors. Without loss of generality, we shall assume that the random field is centered, i.e. $\mathbb{E}[Z(\boldsymbol{x}, t)] = 0, \ \forall (\boldsymbol{x}, t) \in \mathbb{R}^k \times \mathbb{R}$. It will also be assumed that the random field is second-order stationary, so that the covariance function only depends on the space-time lag $(\boldsymbol{h}, u) \in \mathbb{R}^k \times \mathbb{R}$:

$$\mathrm{Cov}(Z(\boldsymbol{x}, t), Z(\boldsymbol{x} + \boldsymbol{h}, t + u)) = C(\boldsymbol{h}, u). \tag{1}$$

The functions $C_S(\boldsymbol{h}) = C(\boldsymbol{h}, 0)$ and $C_T(u) = C(\boldsymbol{0}, u)$ are purely spatial and temporal covariance functions, respectively. It is well-known that $C$ must be a positive semidefinite function over $\mathbb{R}^k \times \mathbb{R}$, see for example Gneiting and Guttorp (2010) and references therein.

A space-time covariance $C$ is separable if it is the product (or the sum) of one spatial and one temporal covariance

**Electronic supplementary material** The online version of this article (https://doi.org/10.1007/s11222-020-09956-4) contains supplementary material, which is available to authorized users.

✉ Denis Allard
denis.allard@inrae.fr

1 Biostatistics and Spatial Processes (BioSP), INRAE, 84914 Avignon, France

2 Department of Mining Engineering, University of Chile, Santiago, Chile

3 Advanced Mining Technology Center, University of Chile, Santiago, Chile

4 Avignon Université, LMA EA 2151, 84000 Avignon, France

5 Centre de Géosciences, MINES ParisTech, PSL University, Paris, France

Published online: 29 June 2020

function. Random fields with separable covariance functions can easily be simulated as the product (or the sum) of a spatial random field constant in time and a temporal random field constant in space. Product of Gaussian random fields are not Gaussian, but a Gaussian distribution can be approximated through the Central Limit Theorem. Although congenial from a mathematical point of view, separability is a simplistic assumption in many applications, which makes separable covariances unable to take into account sophisticated interactions between space and time. Nonseparable space-time covariance functions can be constructed from basic building-blocks of purely spatial and/or temporal covariance functions, taking advantage of the fact that the class of covariance functions is closed under products, convex mixtures and limits. The product-sum (De Iaco et al. 2001) and convex mixture (Ma 2002, 2003) approaches are two such examples. Another straightforward construction is to consider a space-time geometric anisotropy on $\mathbb{R}^{k+1}$, based on an isotropic covariance model and a geometrical transformation (rotation and rescaling) of the coordinates. A more physically oriented construction is to introduce a random velocity vector $\boldsymbol{V} \in \mathbb{R}^d$ and to define $C(\boldsymbol{h}, u) = \mathbb{E}[C_S(\boldsymbol{h} - \boldsymbol{V}u)]$, as proposed in Cox and Isham (1988) for modeling precipitation fields. All these models can easily be simulated, even on very large space-time grids, by combining well-established purely spatial and purely temporal simulation algorithms, see for example Schlather et al. (2015).

Gneiting (2002) proposed a class of fully symmetric space-time covariances that has become one of the standard classes of models for space-time random fields in applications relating to climate variables. It was later extended by Zastavnyi and Porcu (2011). We will refer to this extended class as the Gneiting class or the class of Gneiting-type covariance functions. Using arguments based on normal mixtures, it was generalized by Schlather (2010) to a large class of covariance functions that overlaps with the model proposed in Cox and Isham (1988).

Methods for simulating random fields with a Gneiting covariance function are not numerous. They include the methods based on the Cholesky decomposition of the covariance matrix or on block circulant matrices, as well as variations of turning bands and spectral methods for specific cases. The Cholesky decomposition of the covariance matrix (Davis 1987) is an exact method, but it is well-known that the computational cost to simulate a random field at $n$ space-time locations $\{(\boldsymbol{x}_1, t_1), \ldots, (\boldsymbol{x}_n, t_n)\}$ is $\mathcal{O}(n^3)$. Its application is therefore limited to a few tens of thousands space-time locations only. One way to reduce the computational burden consists in using block circulant matrices and FFT, as introduced by Wood and Chan (1994), Dietrich and Newsam (1997) and Chan and Wood (1999). This approach is fast, but it has limitations: simulations must be performed on regular grids and edge effects are not always well controlled when the correlation function is smooth at the origin or decays slowly. Spectral and turning bands methods, see for example Shinozuka (1971), Matheron (1973) and Chilès and Delfiner (2012, Chapter 7.4) and references therein, are known to be computationally efficient to construct spatial random fields based on the simulation of one-dimensional basic random fields. Moreover, they are scalable, in the sense that, after some initial calculations, the computational burden is proportional to the number of target locations, which furthermore need not be regularly spaced. Two special algorithms for space-time random fields have been proposed in Schlather (2012), see also Schlather et al. (2015, 2020). The first one is an extension of the turning bands method, called turning layers, in which the basic random fields are two-dimensional and are approximated with a discrete (circulant embedding) approach. The second one, known as spectral turning layers, is specifically designed for a Cox–Isham covariance function. A general simulation method that exactly produces a space-time random field with a Gneiting-type covariance function has not been developped yet. In this work, two simulation methods inspired by spectral approaches are presented to fill this gap.

The outline is as follows. Section 2 provides the mathematical background required in the subsequent sections and presents the original and extended Gneiting classes of covariances. Section 3 proposes a spectral approach based on a conditional decomposition of the spectral measure of $C(\boldsymbol{h}, u)$. Section 4 proposes an alternative approach that can be seen as a particular case of the substitution approach presented in Lantuéjoul (2002, Chapter 17). Both approaches are illustrated with synthetic examples. Their pros and cons are compared and discussed in Sect. 5. Finally, Sect. 6 presents conclusions and proposes some perspectives to generalize our approaches.

## 2 Theoretical background

### 2.1 Completely monotone and Bernstein functions

A function on the positive half-line $\varphi(t), t \geq 0$, is said to be completely monotone if it possesses a derivative $\varphi^{(n)}$ for any order $n \in \mathbb{N}$ with $(-1)^n \varphi^{(n)}(t) \geq 0$ for any $t > 0$. By Bernstein's theorem (Bernstein 1929), a continuous completely monotone function can be written as the Laplace transform of a nonnegative measure $\mu$, i.e.

$$\varphi(t) = \int_{\mathbb{R}^+} e^{-rt} \mu(dr). \tag{2}$$

Furthermore, by Schoenberg's theorem (Schoenberg 1938), the radial function

$$\phi(\boldsymbol{h}) = \varphi(|\boldsymbol{h}|^2), \qquad \boldsymbol{h} \in \mathbb{R}^k, \tag{3}$$

where $|\boldsymbol{x}| = \langle \boldsymbol{x}, \boldsymbol{x} \rangle^{1/2}$ denotes the Euclidean norm of vector $\boldsymbol{x}$ and $\langle \boldsymbol{x}, \boldsymbol{y} \rangle$ is the usual scalar product between vectors $\boldsymbol{x}$ and $\boldsymbol{y}$, is a covariance function for any dimension $k \in \mathbb{N} \backslash \{0\}$ if and only if $\varphi(t), t \geq 0$, is a completely monotone function.

Closely related to the completely monotone functions are the Bernstein functions. A function $\psi$ defined on $\mathbb{R}_+$ is a Bernstein function if it is a positive primitive of a completely monotone function. It can be shown (Schilling et al. 2010), Chapter 3) that $\psi$ admits the general expression

$$\psi(t) = a + bt + \int_0^{+\infty} \left(1 - e^{-tx}\right) \nu(dx), \qquad t \in \mathbb{R}_+, \quad (4)$$

where $a, b \geq 0$, and $\nu$ is a positive measure, called Lévy measure, satisfying

$$\int_0^{+\infty} \min(1, x)\, \nu(dx) < +\infty.$$

## 2.2 The original Gneiting class of space-time covariance functions

Even though the applications we have in mind concern space and time, all the theoretical background is actually valid in the $\mathbb{R}^k \times \mathbb{R}^l$ more general setting, with $k$ and $l$ two positive integers. Space-time corresponds to the particular case $l = 1$. The Gneiting class of covariances on $\mathbb{R}^k \times \mathbb{R}^l$ (Gneiting 2002) involves two functions, usually denoted $\varphi$ and $\psi$ and associated with the "spatial" (on $\mathbb{R}^k$) and the "temporal" (on $\mathbb{R}^l$) structures, respectively: Let $\sigma > 0$, $\varphi(t), t \geq 0$, a completely monotone function on $\mathbb{R}_+$ and $\psi(t), t \geq 0$, a Bernstein function. Then,

$$C(\boldsymbol{h}, \boldsymbol{u}) = \frac{\sigma^2}{\psi(|\boldsymbol{u}|^2)^{k/2}} \varphi\left(\frac{|\boldsymbol{h}|^2}{\psi(|\boldsymbol{u}|^2)}\right), (\boldsymbol{h}, \boldsymbol{u}) \in \mathbb{R}^k \times \mathbb{R}^l, \quad (5)$$

is a covariance on $\mathbb{R}^k \times \mathbb{R}^l$. Notice that the function defined in (5) is fully symmetric, i.e. $C(\boldsymbol{h}, \boldsymbol{u}) = C(-\boldsymbol{h}, \boldsymbol{u}) = C(\boldsymbol{h}, -\boldsymbol{u}) = C(-\boldsymbol{h}, -\boldsymbol{u})$. Without loss of generality, we suppose from now on that $C(\boldsymbol{0}, 0) = 1$. Hence, following Gneiting (2002), one can assume that $\sigma^2 = 1, \psi(0) = a = 1$ and that the measure $\mu$ defined in (2) is a probability measure. Unless specified otherwise, we shall also consider throughout that $\mu$ has no atom at 0, which implies that $\lim_{t \to +\infty} \varphi(t) = 0$.

## 2.3 The extended Gneiting class

The temporal structure is parameterized by the function $\psi$. From Gneiting's theorem (Gneiting 2002), a sufficient condition on $\psi$ for the function given in (5) to be a space-time covariance on $\mathbb{R}^k \times \mathbb{R}^l$ is that $\psi(t), t \geq 0$, is a Bernstein function. Zastavnyi and Porcu (2011) established a milder condition on $\psi$, assuming that it is continuous and positive. They showed that the function in (5) is a covariance function for any continuous and completely monotone function $\varphi$ on $[0, +\infty)$ if and only if $\psi$ is conditionally definite negative on $\mathbb{R}^l$, i.e. the function $\gamma$ defined by

$$\gamma(\boldsymbol{u}) := \psi(|\boldsymbol{u}|^2) - \psi(0) = \psi(|\boldsymbol{u}|^2) - 1, \ \boldsymbol{u} \in \mathbb{R}^l,$$

is a variogram on $\mathbb{R}^l$.

Accordingly, the Gneiting covariance (5) belongs to the more general class of functions of the form

$$C(\boldsymbol{h}, \boldsymbol{u}) = \frac{1}{(\gamma(\boldsymbol{u}) + 1)^{k/2}} \varphi\left(\frac{|\boldsymbol{h}|^2}{\gamma(\boldsymbol{u}) + 1}\right), \quad (6)$$

where $\varphi$ is a completely monotone function on $\mathbb{R}_+$ and $\gamma$ a continuous variogram on $\mathbb{R}^l$. From a modeling point of view, the formulation (6) offers much more flexibility than (5), which only allows for isotropic variograms associated with Bernstein functions. In particular, for space-time applications, any one-dimensional variogram is admissible, including nonmonotonic variograms. In the remainder of this work, we will adopt the formulation (6), hereafter referred to as the extended Gneiting class of covariance functions or the class of Gneiting-type covariance functions. The substitution approach presented in Sect. 4 will provide an alternative constructive proof of this result.

In this context, the Lévy representation (4) turns out to be unnecessarily restrictive. Similar to Bochner's theorem for covariance functions, the spectral representation of the variogram (Kolmogorov 1961; Yaglom 1957) states that a continuous function $\gamma \neq 0$ on $\mathbb{R}^l$ is a variogram if and only if

$$\gamma(\boldsymbol{u}) = Q(\boldsymbol{u}) + \int_{\mathbb{R}^l} \left[1 - \cos(\langle \boldsymbol{u}, \boldsymbol{x} \rangle)\right] \mathcal{X}(d\boldsymbol{x}), \quad (7)$$

where $Q(\boldsymbol{u})$ is a nonnegative quadratic form and where the spectral measure $\mathcal{X}$ is positive, symmetric, without an atom at the origin, and satisfies

$$\int_{\mathbb{R}^l} \frac{|\boldsymbol{x}|^2\, \mathcal{X}(d\boldsymbol{x})}{1 + |\boldsymbol{x}|^2} < +\infty. \quad (8)$$

According to Proposition 4.5 in Matheron (1972, Chapter 4), $Q(\boldsymbol{u}) = 0$ if and only if $\gamma(\boldsymbol{u})/|\boldsymbol{u}|^2 \to 0$ as $|\boldsymbol{u}| \to +\infty$. For the sake of simplicity and following common usage in spatial statistics, we will assume throughout that $Q(\boldsymbol{u}) = 0$.

The temporal covariance function associated with (6)

$$C_T(\boldsymbol{u}) = C(\boldsymbol{0}, \boldsymbol{u}) = \left(\gamma(\boldsymbol{u}) + 1\right)^{-k/2} \quad (9)$$

is not necessarily integrable. For example, this occurs when $\gamma(\boldsymbol{u})$ is bounded, since in this case $C_T(\boldsymbol{u})$ does not tend to

zero as $|\boldsymbol{u}|$ tends to infinity. This prevents us using properties of the Fourier transform to establish the existence of a spectral density in all generality. Theorem 1 is a characterization result, which provides a necessary and sufficient condition for the existence of a spectral density for $C$.

**Theorem 1** *Assume that the spectral measure $\mathcal{X}$ is absolutely continuous. Then the covariance $C$ has a spectral density if and only if $\mathcal{X}(\mathbb{R}^l) = \int_{\mathbb{R}^l} \mathcal{X}(d\boldsymbol{x}) = +\infty$.*

This theorem, proven in Appendix A, relies on the conditional decomposition of the spectral measure presented in Sect. 3.1. A Gneiting covariance from the original class, i.e. defined by (5), always admits the representation (7) where $\mathcal{X}$ is an absolutely continuous measure such that $\mathcal{X}(\mathbb{R}^l) = \nu(\mathbb{R}_+)$, where $\nu$ is the Lévy measure defined in (4). Hence Theorem 1 offers a full characterization of the subclass of original Gneiting covariances with a spectral density. It is interesting to make a link between Theorem 1 and bounded variograms. First of all, we establish the following proposition.

**Proposition 1** *A variogram $\gamma(\boldsymbol{u})$ is bounded and thus associated with a covariance function $c(\boldsymbol{u})$ with $\gamma(\boldsymbol{u}) = c(\boldsymbol{0}) - c(\boldsymbol{u})$, if and only if $\mathcal{X}(\mathbb{R}^l) = \int_{\mathbb{R}^l} \mathcal{X}(d\boldsymbol{x}) < +\infty$.*

***Proof*** First, assume that the symmetric measure $\mathcal{X}$ is finite, that is, $\mathcal{X}(\mathbb{R}^l) = A < +\infty$. Then, (7) becomes

$$\gamma(\boldsymbol{u}) = A - \int_{\mathbb{R}^l} \cos(\langle \boldsymbol{u}, \boldsymbol{x}\rangle)\mathcal{X}(d\boldsymbol{x}) = c(\boldsymbol{0}) - c(\boldsymbol{u}),$$

where, by Bochner's theorem, $c(\boldsymbol{u}) = \int_{\mathbb{R}^l} \cos(\langle \boldsymbol{u}, \boldsymbol{x}\rangle)\mathcal{X}(d\boldsymbol{x})$ is a covariance function. The variogram $\gamma$ is thus bounded. Reciprocally, assume that the variogram $\gamma$ is bounded, so that $c(\boldsymbol{u}) = B - \gamma(\boldsymbol{u})$ is a covariance function for some finite value $B$, see Gneiting et al. (2001) for details. Its Bochner representation is $c(\boldsymbol{u}) = \int_{\mathbb{R}^l} \cos(\langle \boldsymbol{u}, \boldsymbol{x}\rangle)\eta(d\boldsymbol{x})$ with $\eta(\mathbb{R}^l) = B$. Hence, $\gamma(\boldsymbol{u}) = B - c(\boldsymbol{u}) = \int_{\mathbb{R}^l}\big(1 - \cos(\langle \boldsymbol{u}, \boldsymbol{x}\rangle)\big)\eta(d\boldsymbol{x})$ and a direct comparison with (7) leads to $\eta(d\boldsymbol{x}) = \mathcal{X}(d\boldsymbol{x})$. Accordingly, $\mathcal{X}(\mathbb{R}^l) = B < +\infty$. □

Putting Theorem 1 and Proposition 1 together, we establish the following: an extended Gneiting covariance function admits a spectral density when $\gamma(\boldsymbol{u})$ is unbounded and its spectral measure $\mathcal{X}$ is absolutely continuous. Examples of pairs $(\gamma, \mathcal{X})$ are given in Table 1.

We now recall Bochner's theorem (Bochner 1955), according to which a continuous function $C$ on $\mathbb{R}^k \times \mathbb{R}^l$ is positive semidefinite, hence a covariance function, if and only if

$$C(\boldsymbol{h}, \boldsymbol{u}) = \int_{\mathbb{R}^k}\int_{\mathbb{R}^l} e^{i\langle \boldsymbol{\omega}, \boldsymbol{h}\rangle + i\langle \boldsymbol{\tau}, \boldsymbol{u}\rangle} F(d\boldsymbol{\omega}, d\boldsymbol{\tau}), \tag{10}$$

where $F$ is a nonnegative finite, symmetric measure on $\mathbb{R}^k \times \mathbb{R}^l$, known as the spectral measure of $C$. Note that since the extended Gneiting class is fully symmetric, the spectral measure $F$ must also be fully symmetric. We finish this Section with a lemma that will be useful for the simulation algorithm proposed in Sect. 4.

**Lemma 1** *The extended Gneiting covariance function defined in (6) can be written as follows:*

$$C(\boldsymbol{h}, \boldsymbol{u}) = \frac{1}{(2\pi)^{k/2}} \int_{\mathbb{R}_+}\int_{\mathbb{R}^k} \cos\left(\sqrt{2r}\,\langle \tilde{\boldsymbol{\omega}}, \boldsymbol{h}\rangle\right) \times \exp\left(-\frac{|\tilde{\boldsymbol{\omega}}|^2(\gamma(\boldsymbol{u}) + 1)}{2}\right) d\tilde{\boldsymbol{\omega}}\, \mu(dr), \tag{11}$$

*where $\mu$ is the measure associated with $\varphi$, as defined in (2).*

***Proof*** The inner integral in the right-hand side of (11) is, up to a multiplicative factor, the Fourier transform at $\sqrt{2r}\,\boldsymbol{h}$ of the function $\tilde{\boldsymbol{\omega}} \mapsto \exp\left(-\frac{|\tilde{\boldsymbol{\omega}}|^2(\gamma(\boldsymbol{u})+1)}{2}\right)$ and is equal to $\left(\frac{2\pi}{\gamma(\boldsymbol{u})+1}\right)^{k/2} \exp\left(-\frac{r|\boldsymbol{h}|^2}{\gamma(\boldsymbol{u})+1}\right)$. Formula (11) then follows from (2) and (6). □

For the sake of clarity, and because most applications are in a space-time context, the presentation will be made in the particular case when $l = 1$. Extensions to the more general case when $l \in \mathbb{N}\backslash\{0\}$ will be discussed in Sect. 5.2.

## 3 Spectral approach

Since we assumed $C(\boldsymbol{0}, 0) = 1$, the spectral measure $F$ defined in (10) is a probability measure. Let $(\boldsymbol{\Omega}^S, \Omega^T)$ be a frequency vector distributed as $F$. Let also $\Phi$ be a random phase that is uniform on $(0, 2\pi)$ and independent of $(\boldsymbol{\Omega}^S, \Omega^T)$. In its most basic form, the spectral method rests on the fact that the random field defined by

$$Z(\boldsymbol{x}, t) = \sqrt{2}\cos(\langle \boldsymbol{\Omega}^S, \boldsymbol{x}\rangle + \Omega^T t + \Phi), \tag{12}$$

has a zero mean and covariance $C$ (Shinozuka 1971). By introducing a multiplicative factor $\sqrt{-2\ln(U)}$, where $U$ is an independent uniform variable on $(0, 1)$, the Box–Muller transformation (Box and Muller 1958) ensures that all marginal distributions of $Z$ are standard Gaussian. To go further and obtain a random field whose finite-dimensional distributions (not only the marginals) are approximately Gaussian, one option is to add and rescale many independent copies of the form (12):

$$\tilde{Z}(\boldsymbol{x}, t) = \sum_{j=1}^{p} \sqrt{\frac{-2\ln(U_j)}{p}} \cos\left(\langle \boldsymbol{\Omega}_j^S, \boldsymbol{x}\rangle + \Omega_j^T t + \Phi_j\right), \tag{13}$$

where $p$ is a positive integer and $\big((\boldsymbol{\Omega}_j^S, \Omega_j^T, \Phi_j, U_j),\ j = 1, \ldots, p\big)$ are independent copies of $(\boldsymbol{\Omega}^S, \Omega^T, \Phi, U)$. Because of the central limit theorem, the finite-dimensional distributions of $\tilde{Z}$ tend to become multivariate Gaussian as $p$ tends to infinity (Lantuéjoul 2002, Chapter 15). Although the joint spectral measure of Gneiting-type covariance functions is not explicitly known, it is possible to simulate the frequency vector $(\boldsymbol{\Omega}^S, \Omega^T)$, as shown in the next subsections.

### 3.1 Sampling the spectral measure

The function $\varphi$ introduced in (2) is a mixture of exponential functions. The mixture parameter $r$ can be seen as deriving from a latent random variable $R$ with distribution $\mu$. Accordingly, a covariance $C$ belonging to the extended Gneiting class (6) is also a mixture of basic covariance functions

$$C(\boldsymbol{h}, u) = \int_0^{+\infty} \frac{1}{\big(1+\gamma(u)\big)^{k/2}} \exp\left(-\frac{r|\boldsymbol{h}|^2}{1+\gamma(u)}\right) \mu(dr) := \int_0^{+\infty} C(\boldsymbol{h}, u \mid r)\, \mu(dr),$$

and their spectral measures are related by the formula

$$F(d\boldsymbol{\omega}, d\tau) = \int_0^{+\infty} F(d\boldsymbol{\omega}, d\tau \mid r)\, \mu(dr).$$

The simulation algorithm proposed hereinafter is conditional on $R$. It relies on the factorization of the spectral measure $F(d\boldsymbol{\omega}, d\tau \mid r)$ into a spatial component and a conditional temporal component:

$$F(d\boldsymbol{\omega}, d\tau \mid r) = F_S(d\boldsymbol{\omega} \mid r)\, F_T(d\tau \mid \boldsymbol{\omega}, r).$$

The following theorem, the proof of which is deferred to Appendix A, makes the expression of these components available via their Fourier transforms.

**Theorem 2** *Consider a Gneiting-type covariance function as given in* (6)*. The two following assertions hold:*

1. *If $\boldsymbol{\Omega}^S(r) \sim F_S(d\boldsymbol{\omega} \mid r)$, then its Fourier transform satisfies*

$$\mathbb{E}\left[e^{i\,\langle \boldsymbol{h}, \boldsymbol{\Omega}^S(r)\rangle}\right] = e^{-r\,|\boldsymbol{h}|^2}. \tag{14}$$

2. *If $\Omega^T(\boldsymbol{\omega}, r) \sim F_T(d\tau \mid \boldsymbol{\omega}, r)$, then its Fourier transform is*

$$\mathbb{E}\left[e^{i\,u\,\Omega^T(\boldsymbol{\omega}, r)}\right] = \exp\left(-\frac{|\boldsymbol{\omega}|^2\,\gamma(u)}{4r}\right) \qquad \boldsymbol{\omega}\text{-a.e.} \tag{15}$$

Algorithm 1, presented below, corresponds to this approach. There, and in the rest of this work, $\mathcal{U}(a, b)$ denotes a uniform random variable on the interval $(a, b)$, $\mathcal{N}_d(m, \boldsymbol{\Sigma})$ denotes the multivariate Gaussian (or normal) distribution with mean $m \in \mathbb{R}^d$ and covariance matrix $\boldsymbol{\Sigma}$ and "$\sim$" means "is distributed as". Equation (14) shows that all the components of $\boldsymbol{\Omega}^S(r)$ are independent and normally distributed with zero mean and variance $2r$. The spatial spectral measure can therefore be easily simulated. The simulation of the conditional temporal spectral measure is more tricky. An adaptation of the shot-noise approach developed by Bondesson (1982) is proposed here. Consider the spectral measure $\mathcal{X}$ of the variogram introduced in Sect. 2.3 (Eqs. (7) and (8)). As shown in Appendix A, it is possible to define a positive and locally integrable function $\theta$ defined on $\mathbb{R}_+$, as well as a family of probability measures $\big(\mathcal{X}_t : t > 0\big)$ on $\mathbb{R}_+$, such that

$$\mathcal{X}(dx) = \int_0^{+\infty} \mathcal{X}_t(dx)\, \theta(t)\, dt. \tag{16}$$

Consider now a Poisson point process $\big(\mathrm{T}_n : n \geq 1\big)$ with intensity function $\lambda(t) = \frac{|\boldsymbol{\omega}|^2\,\theta(t)}{4r}$ on $\mathbb{R}_+$. Let us independently assign to each $\mathrm{T}_n$, a random variable $X_{\mathrm{T}_n}$ distributed according to $\mathcal{X}_{\mathrm{T}_n}$. Then, it is shown in Appendix A that the distribution of the random variable $\sum_{n\geq 1} X_{\mathrm{T}_n}$ coincides with that of $\Omega^T(\boldsymbol{\omega}, r)$.

**Algorithm 1** Spectral simulation of a Gaussian random field with Gneiting-type space-time covariance

**Require:** $k$ and $p$
**Require:** $\mu, \gamma$
**for** $j = 1$ to $p$ **do**
  Simulate $R_j \sim \mu$;
  Simulate $(\boldsymbol{\Omega}_j^S \mid R_j) \sim \sqrt{2R_j}\,\mathcal{N}_k(\boldsymbol{0}, \boldsymbol{I}_k)$;
  Simulate $(\Omega_j^T \mid \boldsymbol{\Omega}_j^S, R_j) \sim F_T$;
  Simulate $\Phi_j \sim \mathcal{U}(0, 2\pi)$;
  Simulate $U_j \sim \mathcal{U}(0, 1)$;
**end for**
For each $(\boldsymbol{x}, t)$, compute $\tilde{Z}(\boldsymbol{x}, t)$ as per (13)

This algorithm is generic, in the sense that it is applicable to any continuous variogram $\gamma$. If the spectral measure of the variogram is integrable, then the number of points of the Poisson process is almost surely finite, which makes the algorithmic implementation possibly exact. The Poisson number may be equal to zero with a nonzero probability. In such a case, the distribution of $\Omega^T(\boldsymbol{\omega}, r)$ has an atom at 0, which is equivalent to saying that $C(\boldsymbol{0}, u)$ does not tend to zero as $u$ tends to infinity. When $\mathcal{X}(\mathbb{R}) = +\infty$, or equivalently from Prop. 1, when $\gamma$ is unbounded, the Poisson point process contains infinitely many points. In this case, the algorithm can only be approximately implemented. Bondesson (1982)

**Table 1** Spectral measures corresponding to selected one-dimensional variograms

| $\gamma(u)$ | $\frac{\mathcal{X}(dx)}{dx}$ | Restriction |
|---|---|---|
| $\lvert u\rvert^\alpha$ | $\frac{-2\,\Gamma(\alpha)}{\Gamma(\alpha/2)\,\Gamma(-\alpha/2)}\,\frac{1}{\lvert x\rvert^{1+\alpha}}$ | $0<\alpha<2$ |
| $\lvert u\rvert - 1 + e^{-\lvert u\rvert}$ | $\frac{1}{\pi}\,\frac{1}{x^2\,(1+x^2)}$ | |
| $\begin{cases}\lvert u\rvert & \text{if } \lvert u\rvert < 1\\ 2\lvert u\rvert - 1 & \text{if } \lvert u\rvert \geq 1\end{cases}$ | $\frac{1}{\pi}\,\frac{1+\cos x}{x^2}$ | |
| $\begin{cases}u^2(3-\lvert u\rvert) & \text{if } \lvert u\rvert < 1\\ 3\lvert u\rvert - 1 & \text{if } \lvert u\rvert \geq 1\end{cases}$ | $\frac{6}{\pi}\,\frac{1-\cos x}{x^4}$ | |
| $\ln(1+u^2)$ | $\frac{\exp(-\lvert x\rvert)}{\lvert x\rvert}$ | |
| $8\sqrt{\pi}\left(\sinh\frac{\operatorname{argsinh} u}{4}\right)^2$ | $\frac{\exp(-\lvert x\rvert)}{\lvert x\rvert^{3/2}}$ | |
| $2\lvert u\rvert\arctan\lvert u\rvert - \ln(1+u^2)$ | $\frac{\exp(-\lvert x\rvert)}{\lvert x\rvert^2}$ | |
| $\frac{8\sqrt{\pi}}{3}\left(1-(1+u^2)^{3/4}\cos\frac{3\arctan u}{2}\right)$ | $\frac{\exp(-\lvert x\rvert)}{\lvert x\rvert^{5/2}}$ | |

made a number of recommendations about the effective number of Poisson points to simulate and the way to approximate the remainder.

To apply this algorithm, the spectral measure of the variogram $\gamma$ is explicitly needed. This is a limitation because such a spectral measure is not always available. Table 1 provides a list of variograms and their associated spectral measures. Note however that "universal" algorithms have been developed to simulate monovariate distributions starting from their Fourier transforms (Devroye 2001; Barabesi and Pratelli 2015), under some conditions on the characteristic functions. These algorithms could be used to simulate directly $\Omega^T(\boldsymbol{\omega}, r)$ without knowing explicitly the spectral measure $\mathcal{X}$. We do not pursue this route in this work since, as we will see in the next subsection, for many variograms, specific simulation algorithms can be conceived. Typical examples include the variogram $\gamma(u) = \left(1+a|u|^\alpha\right)^\beta$ (Gneiting 2002).

## 3.2 Illustrations

Three examples are presented in $\mathbb{R}^2 \times \mathbb{R}$. For the sake of simplicity, they are all based on the same completely monotone function $\varphi(t) = \exp(-rt)$ with $r = 0.01$, but with different variograms $\gamma(u)$. Covariance functions associated with another function $\varphi(t)$ can be simulated as long as one is able to simulate $R$ according to the associated measure $\mu$ in step 2 of Algorithm 1. This point will be further discussed in Sect. 5. All the simulations have been obtained using $p = 5000$ basic cosine waves. They are displayed on a $300 \times 200$ grid with a unit square mesh size, using the same color scale ranging from $-4$ (blue) to $+4$ (red). Six consecutive images, separated by short intervals of 0.2 time units, allow to keep track of the evolution of the large-value zones with time. The first illustration is shown in Fig. 1; the other ones are displayed in the Supplementary Material.

### 3.2.1 First example

The linear variogram $\gamma(u) = b|u|$, with $b > 0$, is certainly one of the simplest variograms that can be considered. Its spectral measure is proportional to the Lebesgue measure. The associated space-time covariance function is

$$C(\boldsymbol{h}, u) = \frac{1}{1+b|u|}\,\exp\left(-\frac{r\,|\boldsymbol{h}|^2}{1+b|u|}\right),$$

which includes a spatial Gaussian covariance and a temporal hyperbolic covariance. The conditional temporal frequencies follow a Cauchy distribution. The simulation of Fig. 1 has been obtained by taking $b = 1$ and $r = 0.01$.

### 3.2.2 Second example

The second example considers the logarithmic variogram $\gamma(u) = \ln\left(1+(au)^2\right)$, with $1/a$ being a temporal scale parameter. The corresponding space-time covariance function is equal to

$$C(\boldsymbol{h}, u) = \frac{1}{1+\ln\left(1+(au)^2\right)}\,\exp\left(-\frac{r\,|\boldsymbol{h}|^2}{1+\ln\left(1+(au)^2\right)}\right).$$

Compared to the first example, the temporal covariance function

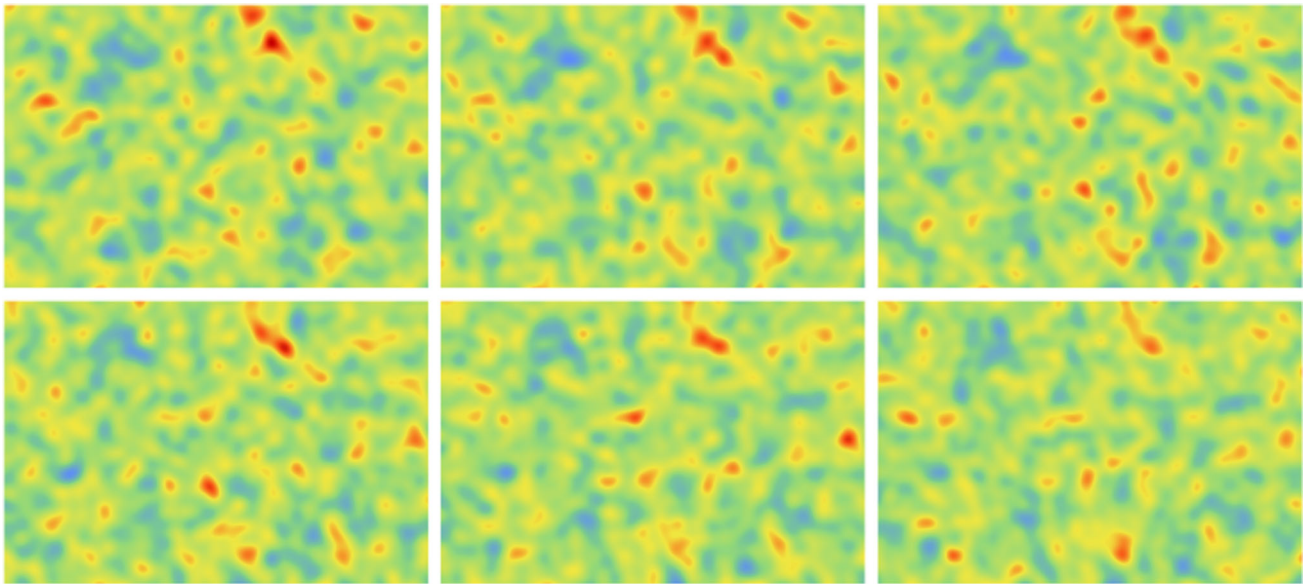

**Fig. 1** Realization of a space-time random field with Gneiting covariance function $C(\boldsymbol{h}, u) = (1 + |u|)^{-1} \exp\left(-0.01|\boldsymbol{h}|^2 (1 + |u|)^{-1}\right)$, displayed on a $300 \times 200$ grid at 6 successive time intervals separated by 0.2 unit (from left to right and from top to bottom)

$$C_T(u) = \frac{1}{1 + \ln\bigl(1 + (au)^2\bigr)}$$

vanishes at infinity at a very slow rate. The spectral measure of $\gamma$ can be derived from the 5th entry of Table 1,

$$\mathcal{X}(dx) = \frac{\exp(-|x|/a)}{|x|}\, dx,$$

which is not integrable in agreement with Proposition 1. To design a simulation algorithm, the generic approach can be applied (see the details in Appendix A), but in the present case a more direct approach is also possible.

Let us start with the Fourier transform (15) of $\Omega^T(\boldsymbol{\omega}, r)$. Replacing $\gamma$ by its expression and putting $\lambda = \frac{|\boldsymbol{\omega}|^2}{4r}$, one obtains

$$\mathbb{E}\left[e^{i\, u\, \Omega^T(\boldsymbol{\omega}, r)}\right] = \left(\frac{1}{1 + (au)^2}\right)^{\lambda}.$$

The right-hand side member of this equation can be seen as the Laplace transform at $(au)^2$ of a gamma distribution with parameter $\lambda$ and index 1. Accordingly, one can write

$$\mathbb{E}\left[e^{i\, u\, \Omega^T(\boldsymbol{\omega}, r)}\right] = \frac{1}{\Gamma(\lambda)} \int_0^{+\infty} e^{-xa^2u^2}\, e^{-x}\, x^{\lambda - 1}\, dx.$$

Since $\exp(-xa^2u^2)$ is the Fourier transform of a centered Gaussian random variable with variance $2a^2x$, it is obtained that the distribution of $\Omega^T(\boldsymbol{\omega}, r)$ is a gamma mixture of Gaussian distributions. The explicit description is detailed in the following algorithm. Below, and in the rest of this work, $\mathcal{G}(\lambda, b)$ denotes the gamma distribution with shape parameter $\lambda$ and scale parameter $b$.

**Algorithm 2** Sampling from the conditional spectral distribution with a logarithmic variogram

**Require:** $a > 0, \lambda = \frac{|\boldsymbol{\omega}|^2}{4r}$
1: Simulate $X \sim \mathcal{G}(\lambda, 1)$ and $Y \sim \mathcal{N}(0, 1)$;
2: Return $\Omega^T(\boldsymbol{\omega}, r) = aY\sqrt{2X}$.

The simulation shown in Fig. 1 of the Supplementary Material has been obtained using this algorithm with $r = 0.01$ and $a = 2.3527$, a value chosen so that the temporal covariance functions of the first two examples take the same value at the time lag 0.2 between successive images.

### 3.2.3 Third example

The third example is the variogram used in Gneiting (2002) for modeling the Irish wind data set, namely $\gamma(u) = (1 + a|u|^{\alpha})^{\beta} - 1$ with $a > 0$, $0 < \alpha \leq 2$ and $0 < \beta \leq 1$, see also Schlather and Moreva (2017) for a detailed presentation of this variogram model. The special case $\alpha = \beta = 1$ corresponds to the first example, whilst the limiting case $\lim_{\beta \to 0} \gamma(u)/\beta$ with $\alpha = 2$ is formally similar to the second example. This model of variogram leads to the space-time covariance function

$$C(\boldsymbol{h}, u) = \frac{1}{(1 + a|u|^{\alpha})^{\beta}} \exp\Bigl(-\frac{r\,|\boldsymbol{h}|^2}{(1 + a|u|^{\alpha})^{\beta}}\Bigr).$$

In particular, the associated temporal covariance $C_T(u) = (a|u|^\alpha + 1)^{-\beta}$ belongs to the Cauchy class (Gneiting and Schlather 2004) and can exhibit a wide range of behaviors. The parameter $\alpha$ governs the behavior at the origin (trajectories become smoother as $\alpha$ increases), while the product $\alpha\beta$ controls the rate of decay at long times (trajectories have a longer memory as $\alpha\beta$ increases). A simulation of a Gneiting model with $r = 0.01$, $a = 1$, $\alpha = 1$ and $\beta = 0.5$ is depicted on Fig. 2 in the Supplementary Material.

The spectral measure of this variogram is unknown, but, here too, the conditional spectral measure can be simulated directly. Let us start again with the Fourier transform (15) of $\Omega^T(\boldsymbol{\omega}, r)$. Replacing $\gamma$ by its expression, and putting $\lambda = \frac{|\boldsymbol{\omega}|^2}{4r}$, the Fourier transform becomes

$$\mathbb{E}\left[e^{i\,u\,\Omega^T(\boldsymbol{\omega},r)}\right] = \exp\left(-\lambda\left((1+a|u|^\alpha)^\beta - 1\right)\right).$$

Up to the factor $\exp(\lambda)$, the right-hand side member is the Laplace transform at $\lambda^{1/\beta}\left(a|u|^\alpha + 1\right)$ of a unilateral stable distribution $\mathcal{S}^+(\beta)$ with stability index $\beta$ (Devroye 2009). Denoting by $f_\beta$ its probability density function, one can write

$$\mathbb{E}\left[e^{i\,u\,\Omega^T(\boldsymbol{\omega},r)}\right] = \exp(\lambda)\int_0^{+\infty} \exp\left(-\lambda^{1/\beta}\left(a|u|^\alpha + 1\right)s\right) f_\beta(s)\,ds.$$

Now, another grouping of factors gives

$$\mathbb{E}\left[e^{i\,u\,\Omega^T(\boldsymbol{\omega},r)}\right] = \int_0^{+\infty} g_\beta(s)\,\exp\left(-\lambda^{1/\beta}a|u|^\alpha s\right)\,ds,$$

where

- $g_\beta(s) = \exp\left(\lambda - \lambda^{1/\beta}\,s\right) f_\beta(s)$ is the density of another distribution, denoted by $\mathcal{S}^+(\beta, \lambda^{1/\beta})$ and called exponentially tilted unilateral stable distribution with stability index $\beta$ and tilting parameter $\lambda^{1/\beta}$, see Devroye (2009) and references therein.
- $\exp\left(-\lambda^{1/\beta}a|u|^\alpha s\right)$ is the Fourier transform at $\left(\lambda^{1/\beta}as\right)^{1/\alpha}$ of a bilateral stable distribution $\mathcal{S}(\alpha)$ with stability index $\alpha$ (Khintchine and Lévy 1936).

It thus appears that the distribution of $\Omega^T(\boldsymbol{\omega}, r)$ is a mixture of bilateral stable distributions. Algorithm 3 makes this assertion more precise.

There remains to see how to simulate those stable distributions. $\mathcal{S}(\alpha)$ can be simulated using the fast algorithm by Chambers et al. (1976) that generalizes the Box–Muller algorithm to simulate normal distributions and has become a standard. Brix (1999) proposes an algorithm to simulate $\mathcal{S}^+(\beta, \lambda^{1/\beta})$ based on a rejection from $\mathcal{S}^+(\beta)$. However, this algorithm may suffer from a high rejection rate for large values of $\lambda^{1/\beta}$. This prompted Devroye (2009) to propose a double rejection technique that possesses a uniform and limited rejection rate.

**Algorithm 3** Sampling from the conditional spectral distribution with Cauchy temporal covariance

**Require:** $a > 0$, $0 < \alpha \leq 2$, $0 < \beta \leq 1$, $\lambda = \frac{|\boldsymbol{\omega}|^2}{4r}$
1: Simulate $S \sim \mathcal{S}^+(\beta, \lambda^{1/\beta})$;
2: Simulate $T \sim \mathcal{S}(\alpha)$;
3: Return $\Omega^T(\boldsymbol{\omega}, r) = T\,(Sa\lambda^{1/\beta})^{1/\alpha}$.

## 4 Substitution approach

### 4.1 Proposal

Instead of simulating a temporal frequency according to the conditional measure $F_T(d\tau \mid \boldsymbol{\omega}, r)$, here we simulate an intrinsic Gaussian random field $W(t)$ on $\mathbb{R}$ with variogram $\gamma$, without making reference to its spectral representation (7). Specifically, consider the random field $Z$ defined in $\mathbb{R}^k \times \mathbb{R}$ as follows:

$$Z(\boldsymbol{x}, t) = \sqrt{-2\ln(U)} \times \cos\left(\sqrt{2R}\,\langle\tilde{\boldsymbol{\Omega}}, \boldsymbol{x}\rangle + \frac{|\tilde{\boldsymbol{\Omega}}|}{\sqrt{2}}W(t) + \Phi\right), \qquad (17)$$

where:

- $R$ is a nonnegative random variable with probability measure $\mu$;
- $\tilde{\boldsymbol{\Omega}}$ is a Gaussian random vector of $k$ independent components with zero mean and unit variance;
- $U$ is a random variable uniformly distributed on $(0, 1)$, independent of $(R, \tilde{\boldsymbol{\Omega}})$;
- $\Phi$ is a random variable, independent of $(R, \tilde{\boldsymbol{\Omega}}, U)$, uniformly distributed on $(0, 2\pi)$;
- $W(t)$, $t \in \mathbb{R}$, is an intrinsic random field on $\mathbb{R}$ with variogram $\gamma$ and Gaussian increments, independent of $(R, \tilde{\boldsymbol{\Omega}}, U, \Phi)$.

**Theorem 3** *The random field $Z$ defined in (17) is second-order stationary in $\mathbb{R}^k \times \mathbb{R}$, with zero mean and Gneiting-type covariance function as given in (6).*

The proof of this theorem is given in Appendix B. The random field $Z(\boldsymbol{x}, t)$ is reminiscent of the spectral turning layers proposed in Schlather (2012) in which one simulates a space-time random field $Z_S(\boldsymbol{x}, t)$ of the form

$$Z_S(\boldsymbol{x}, t) = \sqrt{2}\cos\left(\sqrt{2R}\langle\tilde{\boldsymbol{\Omega}}, \boldsymbol{x} - \boldsymbol{V}t\rangle + \Phi\right), \qquad (18)$$

where $\boldsymbol{V}$ is a random velocity. The important difference lies in the way the temporal component is handled. In $Z_S$, it is a linear function of $t$ with a random slope. The variogram $\gamma(u)$ corresponding to (18) is thus quadratic. In our approach, for any specified variogram $\gamma(u)$, a temporal process $W(t)$ is simulated.

Interestingly, the random field $Z$ defined in (17) is a particular case of a substitution random field, obtained by combining a directing function $D$ with stationary increments in $\mathbb{R}^k \times \mathbb{R}$ and a stationary coding process $X$ in $\mathbb{R}$, as proposed in Lantuéjoul (1991) and Lantuéjoul (2002, Chapter 17), a construction that generalizes the subordination approach introduced by Feller (1966, Chapter 10). Here, the directing function is the sum of a space-dependent linear drift, which has stationary increments in $\mathbb{R}^k$, and a time-dependent random field with stationary increments in $\mathbb{R}$:

$$D(\boldsymbol{x}, t) = \sqrt{2R}\,\langle \tilde{\boldsymbol{\Omega}}, \boldsymbol{x}\rangle + \frac{|\tilde{\boldsymbol{\Omega}}|}{\sqrt{2}} W(t), \qquad (\boldsymbol{x}, t) \in \mathbb{R}^k \times \mathbb{R}.$$

As for the coding process, it is a cosine function in $\mathbb{R}$ with constant frequency $(2\pi)^{-1}$, random phase $\Phi$ uniformly distributed in $(0, 2\pi)$ and random amplitude $\sqrt{-2\ln(U)}$:

$$X(d) = \sqrt{-2\ln(U)}\cos(d + \Phi), \qquad d \in \mathbb{R}.$$

Such a coding process is stationary and has a Gaussian marginal distribution. Because $D$ and $X$ are independent, the substitution random field $Z = X \circ D$ defined in (17) inherits several properties of the coding process (Lantuéjoul 2002, Chapter 17), in particular it is stationary and has the same Gaussian marginal distribution as $X$. The latter property (Gaussian marginal) can also be proven on the basis of the Box–Muller transformation (Box and Muller 1958).

There is actually more, as the coding process is a Gaussian random field in $\mathbb{R}$. This can be proven by observing that any weighted sum of variables $X(d_1), \ldots, X(d_j)$ has a Gaussian distribution, since it can be written under the form $a\sqrt{-2\ln(U)}\cos(b + \Phi)$, with deterministic terms $a$ and $b$ that depend on the chosen weights and time instants $t_1, \ldots, t_j$. In particular, the bivariate distributions of $X$ are bi-Gaussian and have an isofactorial representation with Hermite polynomials as the factors, see Lancaster (1957) and Chilès and Delfiner (2012, Chapter 6). The substitution construction therefore ensures that $Z$ also has bivariate distributions with Hermite polynomials as the factors, which are nothing else than mixtures of bi-Gaussian distributions (Chilès and Delfiner 2012, Chapter 6). Note the similarity of this construction with the substitution models proposed by Matheron (1982) and Emery (2008b).

### 4.2 Simulation algorithm

The random field $Z$ defined in (17) is centered and second-order stationary. Its covariance function belongs to the Gneiting class (6) and its marginal distribution is Gaussian. To obtain a random field whose finite-dimensional distributions are approximately Gaussian, one can simulate a large number of independent random fields $Z_j$, $j = 1, \ldots, p$, as in (17), and set:

$$\tilde{Z}(\boldsymbol{x}, t) = \sum_{j=1}^{p} \sqrt{\frac{-2\ln(U_j)}{p}} \times \cos\left(\sqrt{2R_j}\langle \tilde{\boldsymbol{\Omega}}_j, \boldsymbol{x}\rangle + \frac{|\tilde{\boldsymbol{\Omega}}_j|}{\sqrt{2}} W_j(t) + \Phi_j\right), \qquad (19)$$

where $\{(R_j, \tilde{\boldsymbol{\Omega}}_j, U_j, \Phi_j, W_j) : j = 1, \ldots, p\}$ are independent copies of $(R, \tilde{\boldsymbol{\Omega}}, U, \Phi, W)$.

Algorithm 4 described below can be used for simulating $\tilde{Z}$. The simulation of the intrinsic random field $W_j$ at line 6 can be done by the covariance matrix decomposition method applied to the increment $W_j(t) - W_j(0)$, by fixing $W_j(0) = 0$ and using the nonstationary covariance $\gamma(t) + \gamma(t') - \gamma(t - t')$ (Davis 1987). This is possible as long as the number of time instants considered for the simulation is not too large (less than a few tens of thousands). For larger numbers, other simulation methods are applicable, such as circulant embedding matrices with FFT (Wood and Chan 1994) or the Gibbs propagation algorithm (Arroyo and Emery 2015).

**Algorithm 4** Substitution algorithm

**Require:** $\mu$ and $\gamma(u)$
**Require:** $p$
1: **for** $j = 1$ to $p$ **do**
2: Simulate $R_j \sim \mu$;
3: Simulate $\tilde{\boldsymbol{\Omega}}_j \sim \mathcal{N}_k(\boldsymbol{0}, \boldsymbol{I}_k)$;
4: Simulate $\Phi_j \sim \mathcal{U}(0, 2\pi)$;
5: Simulate $U_j \sim \mathcal{U}(0, 1)$;
6: Simulate an independent intrinsic random field $W_j$ with Gaussian increments and variogram $\gamma(u)$.
7: **end for**
8: Compute the simulated random field at any target location $(\boldsymbol{x}, t) \in \mathbb{R}^k \times \mathbb{R}$ as per (19).

As an illustration, consider the following covariance functions over $\mathbb{R}^2 \times \mathbb{R}$:

$$C_1(\boldsymbol{h}, u) = \frac{1}{\sqrt{1 + |u|}} \exp\left(-\frac{0.01\,|\boldsymbol{h}|^2}{\sqrt{1 + |u|}}\right), \qquad (20)$$

$$C_2(\boldsymbol{h}, u) = \frac{1}{\sqrt{1 + |u|}} \exp\left(-\frac{0.1\,|\boldsymbol{h}|}{\sqrt[4]{1 + |u|}}\right), \qquad (21)$$

which belong to the Gneiting class (6) with $\varphi_1(t) = e^{-0.01t}$, $\varphi_2(t) = e^{-0.1\sqrt{t}}$ and $\gamma(u) = \sqrt{1 + |u|} - 1$. Realizations

of Gaussian random fields possessing these covariances are displayed in Figs. 3 and 4 of the Supplementary Material. The simulation has been obtained with Algorithm 4, by using $p = 5000$ and the covariance matrix decomposition approach to simulate the random fields $W_j$ at the six time instants of interest. Concerning the second example, the probability measure associated with $\varphi_2$ is that of the square root of a Gamma random variable with shape parameter 0.5 (Emery and Lantuéjoul 2006).

## 5 Discussion

### 5.1 Experimental reproduction of the spatio-temporal structure

The reproduction of the covariance structure can be experimentally validated by comparing the sample variograms of a set of realizations with the theoretical variogram $\gamma(\boldsymbol{h}, u) = 1 - C(\boldsymbol{h}, u)$. An example is shown on Fig. 2, where fifty realizations have been generated on a field in $\mathbb{R}^2 \times \mathbb{R}$ with $100 \times 100 \times 100$ nodes with a spatial mesh of $1 \times 1$ and a temporal mesh of 0.2, with the same covariance model given by (20) and $p = 5000$ in both simulation approaches. Each realization was obtained in a matter of minutes on a standard computer, with the nonoptimized code written in GNU Octave's language provided in Supplementary Material. Three spatial and three temporal variograms have been calculated, for time lags $u = 0$, $u = 0.2$ and $u = 1.6$ and space lags $\boldsymbol{h} = (0, 0)$, $\boldsymbol{h} = (6, 6)$ and $\boldsymbol{h} = (10, 10)$, respectively. In all cases, the sample variograms fluctuate without any bias around the expected model, their average over the realizations matching almost perfectly the theoretical variogram, which corroborates the correctness of the proposed algorithms. Interestingly, the spectral approach provides sample variograms that exhibit, for the same number of basic random fields ($p = 5000$) in the sums (13) and (19), slightly higher fluctuations than the substitution approach. This fact can be explained by following arguments in Lantuéjoul (1994): sample variograms of spectral realizations for a given space-time lag $(\boldsymbol{h}, u)$ have a higher variance than those obtained with the substitution approach, although their expectations are the same and equal to $\gamma(\boldsymbol{h}, u)$. Also note the dimple (hole effect) of the temporal variogram associated with the space lag $\boldsymbol{h} = (10, 10)$, a well-known property of the Gneiting model that arises even when the function $\psi$ is monotonic (Kent et al. 2011; Cuevas et al. 2017).

### 5.2 Comparison of the simulation approaches

We presented two approaches for simulating spatio-temporal random fields with a Gneiting-type covariance function, based on two ingredients: a scale mixture argument for the spatial structure and the use of variograms for the temporal structure. Despite algorithmic differences, these two approaches are mathematically very close in the sense that, conditional on the spatial scale $r$, they rely on the decomposition of the spectral measure

$$F(d\boldsymbol{\omega}, d\tau \mid r) = F_S(d\boldsymbol{\omega} \mid r)\, F_T(d\tau \mid \boldsymbol{\omega}, r).$$

Sampling from the marginal spatial spectral measure is common to both approaches, as the random vector $\sqrt{2R}\,\tilde{\boldsymbol{\Omega}}$ used in the substitution approach (17) has the same distribution $\mathcal{N}_k(\boldsymbol{0}, 2R\,\boldsymbol{I}_k)$ as the random vector $\boldsymbol{\Omega}^S(R)$ used in the spectral approach (14). The two methods only differ in the way of handling the temporal dimension.

The spectral approach uses the spectral measure associated with the temporal variogram $\gamma(u)$ in order to sample a conditional temporal frequency. The spectral measure is known for several classes of variogram functions, see Table 1. However, it is not known for some popular temporal structures such as $\gamma(u) = (1 + a|u|^{2\alpha})^{\beta} - 1$. This function was used in Gneiting (2002) and in many other studies implying climate variables, see e.g. Bourotte et al. (2016). In this case however, a specific algorithm was designed, see example 3 above in Sect. 3. A strong advantage of the spectral approach is that it is continuous in $\mathbb{R}^k \times \mathbb{R}$ and requires limited storage space since it only uses $p$ independent copies of random vectors of length $k + 4$. The random field can then be computed at any location $(\boldsymbol{x}, t)$ using (13).

The spectral method can be extended to the simulation in $\mathbb{R}^k \times \mathbb{R}^l$, as it is relies on Theorem 2 that can easily be generalized to that space. In this setting, the simulation of the spatial density remains unchanged; conditional upon $(\boldsymbol{\Omega}^S, R)$, the "temporal" frequency vector $\boldsymbol{\Omega}^T = (\Omega_1^T, \ldots, \Omega_l^T)$ is still an infinitely divisible random vector. The only difficulty is the simulation of multivariate infinitely divisible distributions. But, as it was the case for $l = 1$, a case-by-case approach can be considered.

In the substitution approach, one simulates a pure spatial drift and a temporal intrinsic random field $W(t)$ with Gaussian increments and project them onto $(\boldsymbol{x}, t)$ using a cosine function, as in (17). One advantage of using a standardized Gaussian random vector $\tilde{\boldsymbol{\Omega}}$ instead of a vector $\boldsymbol{\Omega}^S(R)$ with components of variance $2R$ is the possibility to apply the algorithm even if $R$ is zero, which happens with a non-zero probability if the measure $\mu$ defined in (2) has an atom at 0. Although this case has been excluded in the presentation of both simulation approaches, it would not imply any change in the proposal in Sect. 4 and the demonstration in Appendix B. Another advantage of the substitution approach is that it is absolutely generic, in the sense that the spectral measure of $\gamma(u)$ does not need to be known. Several discrete simulation algorithms such as the covariance matrix decomposition, the circulant embedding or the Gibbs propagation are possible

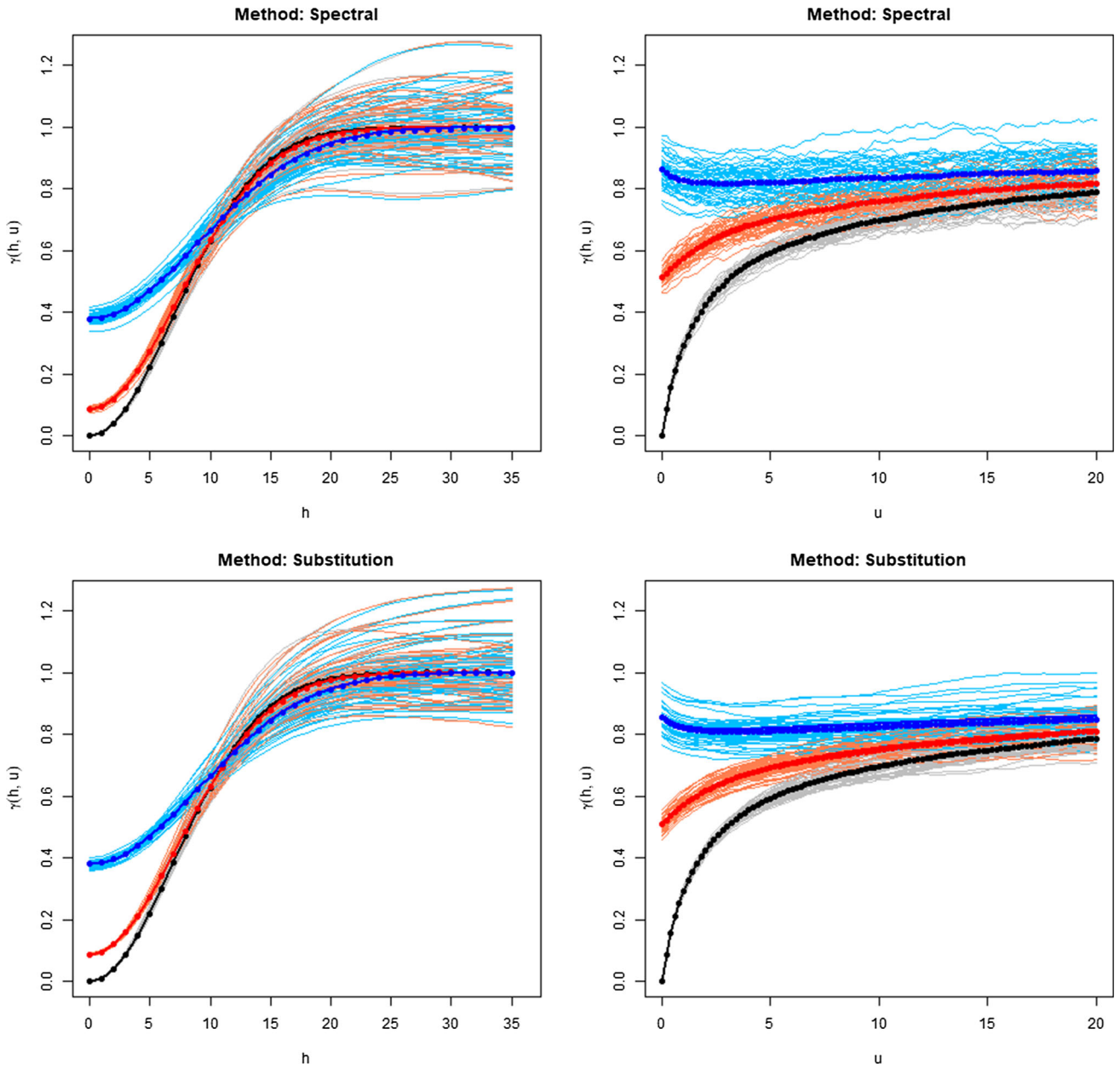


**Fig. 2** Spatial and temporal sample variograms (solid thin lines) for fifty realizations of the model defined by (20) obtained with the spectral approach (top) and the substitution approach (bottom) on a $100 \times 100 \times 100$ domain of $\mathbb{R}^2 \times \mathbb{R}$ with spatial mesh $1 \times 1$ and temporal mesh 0.2. Three spatial variograms are drawn in the left column, associated with $u = 0$ (black), $u = 0.2$ (red) and $u = 1.6$ (blue). Three temporal variograms are drawn in the right column, associated with $\boldsymbol{h} = (0, 0)$ (black), $\boldsymbol{h} = (6, 6)$ (red) and $\boldsymbol{h} = (10, 10)$ (blue). In each case, the mean of the sample variogram (dots) and the theoretical variograms (solid thick lines) are superimposed. (Color figure online)

in order to simulate $W(t)$, as already pointed out in Sect. 3. These algorithms are applicable not only in $\mathbb{R}$, but also in $\mathbb{R}^l$ with $l > 1$, which makes straightforward the extension of the presented approach to $\mathbb{R}^k \times \mathbb{R}^l$. The only difference lies in that the intrinsic random field $W$ is now defined on $\mathbb{R}^l$, and so is its variogram $\gamma(\boldsymbol{u})$. Simulating a random field $W$ on $\mathbb{R}^l$ is, however, more difficult than on $\mathbb{R}$, essentially because the number of points targeted for simulation usually increases with $l$. Note also that, in this approach, $\gamma$ can be any variogram on $\mathbb{R}^l$, which proves that this is a sufficient condition for the Gneiting covariance in (6) to be a valid model. The assumption of continuity of $\gamma$ is not even needed: variograms with a nugget effect, which do not have a spectral representation, can be considered in the construction by substitution.

The disadvantage is that the random field will be simulated only at those temporal coordinates where $W(t)$ has

been simulated. If $n_T$ denotes the number of such temporal coordinates, then the simulation requires $n_T + p(k+3)$ values to be stored. Although this is uncommon in practice, a huge number of temporal coordinates (say, $n_T > 10^6$) may make the computational requirements prohibitive for the aforementioned discrete algorithms.

Whether the spectral or the substitution algorithm is chosen for simulation, two additional points deserve attention for practical implementation:

- Choice of the number $p$ of basic cosine waves: as a rule of thumb, several thousands waves are usually recommended, although fewer waves can be used when the covariance function is smooth near the origin, see Lantuéjoul (1994), Lantuéjoul (2002, Chapter 15), Emery and Lantuéjoul (2006), Emery (2008a) and Schlather (2012);
- Determination of the measure $\mu$ and design of an algorithm to simulate $R_1, \ldots, R_p \sim \mu$: many examples of measures associated with common completely monotone functions are available in Oberhettinger and Badii (1973, Chapters 1–2), while numerous algorithms for simulating real-valued random variables are described in Devroye (1986, Chapters 2–10). A nontrivial example where $\mu$ is not a Dirac measure centered on a fixed value $r$ has been presented in Sect. 4.2 for the exponential function (21).

As a guideline for practitioners, the main computational properties and conditions of application of the proposed algorithms, as well as those of other two well-known generic algorithms (Cholesky decomposition of the covariance matrix and circulant embedding simulation), are summarized in Table 2. Of particular interest is the computational complexity, much lower for the former than for the latter two algorithms, and the fact that calculations can be parallelized since the projection onto target locations can be computed independently. This makes the simulation extremely fast (in a matter of seconds or minutes for the examples presented in Sects. 3.2, 4.2 and 5.1).

## 6 Conclusions and perspectives

Two algorithms have been presented to simulate space-time random fields with nonseparable covariance belonging to the Gneiting class. The first one relies on a spectral decomposition of the covariance and constructs the simulated random field as a weighted sum of cosine waves with random frequencies and phases. In the second algorithm, an intrinsic time-dependent random field is substituted for the temporal frequency, yielding another representation of the simulated random field as a mixture of cosine waves. The proposed algorithms have been tested and validated through synthetic case studies. Their computational requirements are affordable in terms of both memory storage and CPU time. Memory requirement is proportional to the number of cosine waves, to the order of a few thousands. As for CPU time, after an overhead computation consisting in generating a few thousands random variables (which is a matter of a few seconds), the number of floating point operations is proportional to the number of target space-time locations, whether being in $\mathbb{R}^2 \times \mathbb{R}$ or $\mathbb{R}^k \times \mathbb{R}$ with $k > 2$. Also, the algorithms can be adapted to the simulation of random fields in $\mathbb{R}^k \times \mathbb{R}^l$ with $l > 1$. In this case also, up to the overhead computation, the CPU time is proportional to the number of target locations.

This work paves the road to many possible extensions. Rather straightforward extensions include the simulation of multivariate space-time random fields based on the Gneiting class such as those proposed in Bourotte et al. (2016), more general models based on normal mixtures (Schlather 2010) and the simulation of random fields on spheres cross time with covariance models similar to the Gneiting class,

**Table 2** Comparison of simulation algorithms

| Algorithm | Numerical complexity | Spatial field | Temporal field | Remarks |
|---|---|---|---|---|
| Spectral | $\mathcal{O}(n)$ | Continuous | Continuous | (1) |
| Substitution | $\mathcal{O}(n)$ | Continuous | Discrete | (2) |
| Cholesky decomposition | $\mathcal{O}(n^3)$ | Discrete | Discrete | (3) |
| Circulant embedding | $\mathcal{O}(n \ln(n))$ | Discrete | Discrete | (4) |

(1) Applicable when, (i) the probability measure $\mu$ has no atom at 0 and is simulatable, and (ii) the variogram $\gamma$ is continuous with known spectral measure, or the conditional temporal frequency is simulatable starting from its Fourier transform (15); allows an unlimited number of target space-time locations due to the continuous nature of the algorithm.
(2) Applicable when the probability measure $\mu$ is simulatable and the number of target time instants is limited, say less than $10^6$; unlimited number of spatial locations.
(3) Applicable to a limited number ($< 10^5$) of target space-time locations due to CPU time and memory storage requirements.
(4) Applicable to a limited number ($< 10^6$) of target space-time locations forming a regular grid due to CPU time and memory storage requirements; approximate covariance reproduction due to edge effects

but involving Stieltjes functions instead of Bernstein functions, see White and Porcu (2019). Other nonseparable models could also be simulated using at least one of the approaches presented here, including models proposed in Ma (2003). Spatio-temporal random fields derived from SPDEs are characterized through their spectral measures, see Carrizo-Vergara et al. (2018) for a general presentation of these models. Simulating such fields could in some cases be performed using our spectral approach under the condition that one is able to simulate from the spectral measure, which requires further scrutiny. An interesting feature of these models is that, contrarily to the Gneiting class, they are not necessarily fully symmetric and that the marginal covariance function $C_S$ can include nonmonotonic behaviors.

**Acknowledgements** Denis Allard and Christian Lantuéjoul acknowledge support of the RESSTE network funded by the Applied Mathematics and Informatics division of INRA. Xavier Emery acknowledges the support of Grant CONICYT PIA AFB180004 (AMTC) from the National Agency for Research and Development of Chile. We are grateful to three anonymous reviewers for their very careful reading and the many valuable comments that helped to improve the manuscript.

## A Proofs for the spectral approach

### A.1 Proof of Theorem 1

We use the notations defined in Sect. 3. Substituting (7) in (15), one obtains

$$\begin{aligned}
&\mathbb{E}\left[e^{i\,u\,\Omega^T(\boldsymbol{\omega},r)}\right] \\
&\quad = \exp\big(-\lambda(\boldsymbol{\omega},r)\gamma(u)\big) \\
&\quad = \exp\left(-\lambda(\boldsymbol{\omega},r)\int_{\mathbb{R}}(1-\cos(ux))\,\mathcal{X}(dx)\right) \\
&\quad = \exp\left(\lambda(\boldsymbol{\omega},r)\int_{\mathbb{R}}\left(e^{iux}-1-\frac{iux}{1+x^2}\right)\mathcal{X}(dx)\right), \\
&\quad u\in\mathbb{R}, \qquad (22)
\end{aligned}$$

where $\lambda(\boldsymbol{\omega},r)=\frac{|\boldsymbol{\omega}|^2}{4r}$ and where the last equality stems from the symmetry of $\mathcal{X}$ and the integrability condition (8). Therefore, the distribution $F_T(d\tau \mid \boldsymbol{\omega},r)$ is an infinitely divisible distribution with Lévy measure $\nu_{\boldsymbol{\omega},r}=\lambda(\boldsymbol{\omega},r)\mathcal{X}$.

Assume first that $\mathcal{X}(\mathbb{R})=+\infty$. In this case, $\nu_{\boldsymbol{\omega},r}(\mathbb{R})=+\infty$ for $\boldsymbol{\omega}\neq 0$ and the Lévy measure $\nu_{\boldsymbol{\omega},r}$ is absolutely continuous, since $\mathcal{X}$ is absolutely continuous. Then, by applying Lemma 1 of Sato (1982) the infinitely divisible distribution $F_T(d\tau \mid \boldsymbol{\omega},r)$ is absolutely continuous for $\boldsymbol{\omega}\neq 0$ and for a.e. $\boldsymbol{\omega}$. As a consequence, since $F_S(d\boldsymbol{\omega}\mid r)$ is also absolutely continuous, it follows that

$$F(d\boldsymbol{\omega},d\tau)=\int_0^{+\infty}F_S(d\boldsymbol{\omega}\mid r)F_T(d\tau\mid\boldsymbol{\omega},r)\mu(dr)$$

is absolutely continuous.

Let us now assume $\vartheta=\mathcal{X}(\mathbb{R})<+\infty$. In this case, (22) can be rewritten as

$$\mathbb{E}\left[e^{i\,u\,\Omega^T(\boldsymbol{\omega},r)}\right]=\exp\left(\lambda(\boldsymbol{\omega},r)\int_{\mathbb{R}}\left(e^{iux}-1\right)\mathcal{X}(dx)\right),$$

by symmetry of the finite measure $\mathcal{X}$. Since $0<\vartheta<+\infty$, $\Omega^T(\boldsymbol{\omega},r)$ has a compound Poisson distribution with $\mathbb{P}\big(\Omega^T(\boldsymbol{\omega},r)=0)\big)=\exp\big(-\vartheta\lambda(\boldsymbol{\omega},r)\big)$, which implies that

$$\mathbb{P}\left(\Omega^T=0\right)=\mathbb{E}\left[\exp\left(-\frac{\vartheta|\boldsymbol{\Omega}^S|^2}{4R}\right)\right]>0.$$

In conclusion, when $\vartheta<+\infty$, the distribution of $\Omega^T$ has an atom at 0. Hence, $F$ is not absolutely continuous in this case.

### A.2 Proof of Theorem 2

Recall that

$$\begin{aligned}
C(\boldsymbol{h},u\mid r)&=\frac{1}{\big(\gamma(u)+1\big)^{k/2}}\exp\left(-\frac{r|\boldsymbol{h}|^2}{\gamma(u)+1}\right)\\
&:=\int_{\mathbb{R}^k}\int_{\mathbb{R}}e^{i\langle\boldsymbol{h},\boldsymbol{\omega}\rangle+iu\tau}\,F_T(d\tau\mid\boldsymbol{\omega},r)\,F_S(d\boldsymbol{\omega}\mid r). \qquad (23)
\end{aligned}$$

If $u=0$, then

$$C(\boldsymbol{h},0\mid r)=\exp\left(-r|\boldsymbol{h}|^2\right):=\int_{\mathbb{R}^k}e^{i\langle\boldsymbol{h},\boldsymbol{\omega}\rangle}\,F_S(d\boldsymbol{\omega}\mid r),$$

which is nothing but (14). This shows that $F_S$ possesses the density

$$f_S(\boldsymbol{\omega}\mid r)=\frac{1}{(4\pi r)^{k/2}}\exp\left(-\frac{|\boldsymbol{\omega}|^2}{4r}\right). \qquad (24)$$

Plugging (24) into (23), one obtains

$$\begin{aligned}
C(\boldsymbol{h},u\mid r)=&\frac{1}{(4\pi r)^{k/2}}\int_{\mathbb{R}^k}e^{i\langle\boldsymbol{h},\boldsymbol{\omega}\rangle}\\
&\times\exp\left(-\frac{|\boldsymbol{\omega}|^2}{4r}\right)\int_{\mathbb{R}}e^{iu\tau}\,F_T(d\tau\mid\boldsymbol{\omega},r)\,d\boldsymbol{\omega}. \qquad (25)
\end{aligned}$$

On the other hand, up to a multiplicative factor, the function $\boldsymbol{\omega}\mapsto\exp\big(-r|\boldsymbol{h}|^2/(\gamma(u)+1)\big)$ is the Fourier transform of a Gaussian random vector:

$$C(\boldsymbol{h}, u \mid r) = \frac{1}{(4\pi r)^{k/2}} \int_{\mathbb{R}^k} e^{i\langle \boldsymbol{h}, \boldsymbol{\omega}\rangle} \times \exp\left(-\frac{|\boldsymbol{\omega}|^2 (\gamma(u)+1)}{4r}\right) d\boldsymbol{\omega}. \quad (26)$$

Comparing (25) and (26), the injectivity of the Fourier transform implies

$$\exp\left(-\frac{|\boldsymbol{\omega}|^2}{4r}\right) \int_{\mathbb{R}} e^{iu\tau} F_T(d\tau \mid \boldsymbol{\omega}, r) = \exp\left(-\frac{|\boldsymbol{\omega}|^2 (\gamma(u)+1)}{4r}\right) \quad \boldsymbol{\omega}\text{-a.e.},$$

or equivalently

$$\int_{\mathbb{R}} e^{iu\tau} F_T(d\tau \mid \boldsymbol{\omega}, r) = \exp\left(-\frac{|\boldsymbol{\omega}|^2 \gamma(u)}{4r}\right) \quad \boldsymbol{\omega}\text{-a.e.},$$

which is precisely (15). □

### A.3 On the generic approach

The aim of this section is to show that $\sum_{n\geq 1} X_{\mathrm{T}_n}$ and $\Omega^T(\boldsymbol{\omega}, r)$ have the same distribution. This is done by comparing their Fourier transforms. Remind that the spectral measure of the variogram is positive, symmetric, without an atom at the origin, and satisfies the integrability property

$$\int_{\mathbb{R}} \frac{x^2 \mathcal{X}(dx)}{1+x^2} = A < +\infty. \quad (27)$$

Let us start with

$$\mathcal{X}(dx) = \int_{\mathbb{R}_+} \exp\left(-t\frac{x^2}{1+x^2}\right) \frac{x^2 \mathcal{X}(dx)}{1+x^2}\, dt.$$

Because of (27), the positive function $\theta$ defined on $\mathbb{R}_+$ by

$$\theta(t) = \int_{\mathbb{R}} \exp\left(-t\frac{x^2}{1+x^2}\right) \frac{x^2 \mathcal{X}(dx)}{1+x^2}$$

is upper bounded by $A$. It follows that, for each $t > 0$, the measure

$$\mathcal{X}_t(dx) = \frac{1}{\theta(t)} \exp\left(-t\frac{x^2}{1+x^2}\right) \frac{x^2 \mathcal{X}(dx)}{1+x^2}$$

is a probability measure on $\mathbb{R}$. This measure is symmetric, and satisfies

$$\mathcal{X}(dx) = \int_{\mathbb{R}_+} \mathcal{X}_t(dx)\, \theta(t)\, dt. \quad (28)$$

Consider now a Poisson point process $(\mathrm{T}_n : n \geq 1)$ with intensity $\lambda(t) = \lambda\, \theta(t)$ on $\mathbb{R}_+$ ($\lambda$ is put here as a short notation for $\frac{|\boldsymbol{\omega}|^2}{4r}$). Since $\theta\ \lambda(t)$ is upper bounded by $\lambda A$, this process has no accumulation point. Consider also a family $(X_t : t \in \mathbb{R}_+)$ of independent random variables, with $X_t$ being distributed as $\mathcal{X}_t$. Because $\mathcal{X}_t$ is symmetric, the Fourier transform of $X_t$ can be written as

$$\mathbb{E}\big[\exp(iuX_t)\big] = \int_{\mathbb{R}} \cos(ux)\, \mathcal{X}_t(dx). \quad (29)$$

In what follows, we calculate the Fourier transform of $\mathrm{T} = \sum_{n\geq 1} X_{\mathrm{T}_n}$. Denoting by $\Lambda(t_0)$ the integral of $\lambda(t)$ on $]0, t_0[$, we have

$$\begin{aligned}
&\mathbb{E}\big[\exp(iu\mathrm{T})\big] \\
&= \lim_{t_0 \longrightarrow +\infty} \sum_{n=0}^{+\infty} \exp\big(-\Lambda(t_0)\big) \frac{\Lambda^n(t_0)}{n!} \\
&\quad \times \left[\int_0^{t_0} \frac{\lambda(t)}{\Lambda(t_0)} \mathbb{E}\big[\exp(iuX_t)\big]\, dt\right]^n \\
&= \lim_{t_0 \longrightarrow +\infty} \exp\left(\int_0^{t_0} \mathbb{E}\big[\exp(iuX_t) - 1\big]\, \lambda(t)\, dt\right) \\
&= \exp\left(\int_0^{+\infty} \mathbb{E}\big[\exp(iuX_t) - 1\big]\, \lambda(t)\, dt\right).
\end{aligned}$$

This implies, owing to (29)

$$\mathbb{E}\big[\exp(iu\mathrm{T})\big] = \exp\left(\int_0^{+\infty} \int_{\mathbb{R}} \big[\cos(ux) - 1\big]\, \mathcal{X}_t(dx)\, \lambda(t)\, dt\right).$$

Permuting the integrals and replacing $\lambda(t)$ by its expression, we obtain

$$\mathbb{E}\big[\exp(iu\mathrm{T})\big] = \exp\left(\frac{|\boldsymbol{\omega}|^2}{4r} \int_{\mathbb{R}} \big[\cos(ux) - 1\big]\, \mathcal{X}(dx)\right).$$

Finally, the spectral representation (7) of $\gamma$ gives

$$\mathbb{E}\big[\exp(iu\mathrm{T})\big] = \exp\left(-\frac{|\boldsymbol{\omega}|^2}{4r}\gamma(u)\right),$$

which is precisely the Fourier transform (15) of $\Omega^T(\boldsymbol{\omega}, r)$. □

### A.4 Implementing the generic approach for logarithmic variograms

The construction of $\theta$ and $\mathcal{X}_t$ proposed in Appendix A.3 is not necessarily unique. Starting from

$$\begin{aligned}
\mathcal{X}(dx) &= \frac{\exp(-a|x|)}{|x|\, \ln a^2} \\
&= \frac{1}{\ln a^2} \int_a^{+\infty} \exp\big(-t\,|x|\big)\, dt,
\end{aligned}$$

it appears that a possible decomposition such as (16) can be obtained by taking

$$\theta(t) = \frac{2}{t\,\ln a^2}\,1_{t\geq a} = \frac{1}{t\,\ln a}\,1_{t\geq a}$$

and

$$\mathcal{X}_t(dx) = \frac{1}{2}t\,e^{-t|x|}\,dx, \qquad t > a.$$

Consider now a Poisson point process $\big(\mathrm{T}_n : n \geq 1\big)$ on $\mathbb{R}_+$ with intensity function

$$\lambda(t) = \frac{|\boldsymbol{\omega}|^2}{4\,r}\,\theta(t) := \frac{\lambda}{t}\,1_{t\geq a}.$$

A simple approach to simulate a nonhomogeneous Poisson point process is recommended by Devroye (1986, Chapter 6). It consists in calculating the inverse of the primitive of the intensity function $\lambda(t)$ that vanishes at $a$, i.e. $\Lambda(t) = \lambda\,\ln(t/a)$, at the points of a homogeneous Poisson process with a unit intensity on the positive half-line, as shown in Fig. 3.

In this figure, the $U_i$'s are independent standard uniform variables and are related to the Poisson time $\mathrm{T}_n$ by the formula $\Lambda(\mathrm{T}_n) = \lambda\,\ln(\mathrm{T}_n/a) = -\ln\big(U_1\cdots U_n\big)$, which gives

$$\mathrm{T}_n = \frac{a}{(U_1\cdots U_n)^{1/\lambda}}. \tag{30}$$

Now, recall that $\Omega^T(\boldsymbol{\omega}, r)$ has the same distribution as $\sum_{n=1}^{+\infty} X_{\mathrm{T}_n}$, where each $X_t$ is distributed as $\mathcal{X}_t$. Because the $X_t$'s are independent, we have

$$\mathrm{Var}\Big[\sum_{n\geq 1} X_{\mathrm{T}_n}\Big] = \sum_{n\geq 1}\mathrm{Var}\big[X_{\mathrm{T}_n}\big].$$

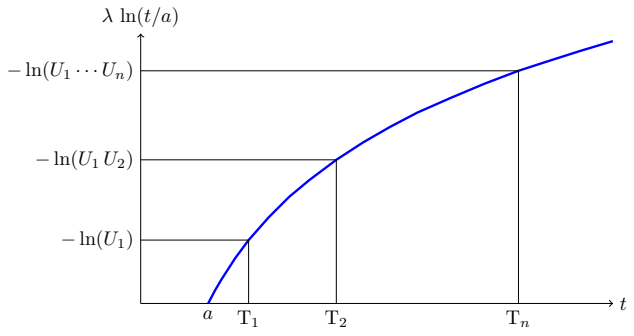


**Fig. 3** Simulation of a nonhomogeneous Poisson point process by inversion of a homogeneous Poisson process with a unit intensity

Moreover, (30) implies

$$\mathrm{Var}\big[X_{\mathrm{T}_n}\big] = \mathbb{E}\Big[\mathrm{Var}\big[X_{\mathrm{T}_n}|\mathrm{T}_n\big]\Big] = \mathbb{E}\Big[\frac{2}{\mathrm{T}_n^2}\Big]$$
$$= \frac{2}{a^2}\,\mathbb{E}\Big[(U_1\cdots U_n)^{2\lambda}\Big] = \frac{2}{a^2}\,\Big(\frac{\lambda}{\lambda+2}\Big)^n.$$

Consequently

$$\mathrm{Var}\Big[\sum_{n\geq 1} X_{\mathrm{T}_n}\Big] = \frac{2}{a^2}\sum_{n\geq 1}\Big(\frac{\lambda}{\lambda+2}\Big)^n = \frac{\lambda}{a^2}.$$

Similarly, if the series is truncated at order $n_0$, then the same calculation leads to the residual variance

$$\mathrm{Var}\Big[\sum_{n\geq n_0+1} X_{\mathrm{T}_n}\Big] = \frac{2}{a^2}\sum_{n\geq n_0+1}\Big(\frac{\lambda}{\lambda+2}\Big)^n$$
$$= \Big(\frac{\lambda}{\lambda+2}\Big)^{n_0}\frac{\lambda}{a^2}.$$

Let $\varepsilon > 0$ be arbitrarily small. From the previous calculations, it follows that

$$\frac{\mathrm{Var}\Big[\sum_{n\geq n_0+1} X_{\mathrm{T}_n}\Big]}{\mathrm{Var}\Big[\sum_{n\geq 1} X_{\mathrm{T}_n}\Big]} < \varepsilon \iff \Big(\frac{\lambda}{\lambda+2}\Big)^{n_0} < \varepsilon$$
$$\iff n_0 > \frac{-\ln\epsilon}{\ln(1+2/\lambda)}.$$

□

## B Proofs for the substitution approach

### Proof of Theorem 3

For $(\boldsymbol{x}, t) \in \mathbb{R}^k \times \mathbb{R}$, $Z(\boldsymbol{x}, t)$ conditional on $(R, \tilde{\boldsymbol{\Omega}}, U, W)$ (i.e. only letting $\Phi$ vary randomly) has a zero expectation, insofar as it is proportional to the cosine of a random variable uniformly distributed on an interval of length $2\pi$. The prior expectation of $Z(\boldsymbol{x}, t)$ is therefore zero:

$$\mathbb{E}[Z(\boldsymbol{x}, \boldsymbol{t})] = \mathbb{E}[\mathbb{E}[Z(\boldsymbol{x}, t) \mid R, \tilde{\boldsymbol{\Omega}}, U, W]] = 0.$$

Let us now calculate the covariance between the random variables $Z(\boldsymbol{x}, t)$ and $Z(\boldsymbol{x}', t')$, with $(\boldsymbol{x}, t) \in \mathbb{R}^k \times \mathbb{R}$ and $(\boldsymbol{x}', t') \in \mathbb{R}^k \times \mathbb{R}$:

$$\mathbb{E}[Z(\boldsymbol{x}, t)Z(\boldsymbol{x}', t')]$$
$$= 2\mathbb{E}\Big[-\ln(U)\cos\Big(\sqrt{2R}\,\langle\tilde{\boldsymbol{\Omega}}, \boldsymbol{x}\rangle + \frac{|\tilde{\boldsymbol{\Omega}}|}{\sqrt{2}}W(t) + \Phi\Big)$$
$$\times\cos\Big(\sqrt{2R}\,\langle\tilde{\boldsymbol{\Omega}}, \boldsymbol{x}'\rangle + \frac{|\tilde{\boldsymbol{\Omega}}|}{\sqrt{2}}W(t') + \Phi\Big)\Big]$$

$$= 2\mathbb{E}\Big[\cos\left(\sqrt{2R}\,\langle\tilde{\boldsymbol{\Omega}},\boldsymbol{x}\rangle + \frac{|\tilde{\boldsymbol{\Omega}}|}{\sqrt{2}}W(t) + \Phi\right)$$
$$\times \cos\left(\sqrt{2R}\,\langle\tilde{\boldsymbol{\Omega}},\boldsymbol{x}'\rangle + \frac{|\tilde{\boldsymbol{\Omega}}|}{\sqrt{2}}W(t') + \Phi\right)\Big].$$

The last equality stems from the fact that $-\ln(U)$ is an exponential random variable with mean 1 and is independent of $(R, \tilde{\boldsymbol{\Omega}}, W)$. Using the product-to-sum trigonometric identities, one can write the product of cosines as half the sum of two cosines, namely:

- the cosine of the difference: $\cos\left(\sqrt{2R}\,\langle\tilde{\boldsymbol{\Omega}},\boldsymbol{x}-\boldsymbol{x}'\rangle + \frac{|\tilde{\boldsymbol{\Omega}}|}{\sqrt{2}}(W(t)-W(t'))\right)$
- the cosine of the sum: $\cos\left(\sqrt{2R}\,\langle\tilde{\boldsymbol{\Omega}},\boldsymbol{x}+\boldsymbol{x}'\rangle + \frac{|\tilde{\boldsymbol{\Omega}}|}{\sqrt{2}}(W(t)+W(t')) + 2\Phi\right)$.

However, because $\Phi$ is uniformly distributed on $(0, 2\pi)$ and independent of $(R, \tilde{\boldsymbol{\Omega}}, W)$, the expectation of the cosine of the sum is 0. It remains

$$\mathbb{E}[Z(\boldsymbol{x},t)Z(\boldsymbol{x}',t')]$$
$$= \mathbb{E}\Big[\cos\left(\sqrt{2R}\,\langle\tilde{\boldsymbol{\Omega}},\boldsymbol{x}-\boldsymbol{x}'\rangle + \frac{|\tilde{\boldsymbol{\Omega}}|}{\sqrt{2}}(W(t)-W(t'))\right)\Big].$$

The increment $W(t) - W(t')$ is a Gaussian random variable with zero mean and variance $2\gamma(t-t')$ and is independent of $(R, \tilde{\boldsymbol{\Omega}})$, i.e.:

$$W(t) - W(t') = \sqrt{2\gamma(t-t')}Y,$$

with $Y \sim \mathcal{N}(0,1)$ independent of $(R, \tilde{\boldsymbol{\Omega}})$. Defining $\boldsymbol{h} = \boldsymbol{x}-\boldsymbol{x}'$ and $u = t-t'$ and denoting by $g$ the standard Gaussian probability density, one therefore obtains:

$$\mathbb{E}[Z(\boldsymbol{x},t)Z(\boldsymbol{x}',t')]$$
$$= \int_{\mathbb{R}_+}\int_{\mathbb{R}^k}\int_{\mathbb{R}} \cos\left(\sqrt{2r}\,\langle\tilde{\boldsymbol{\omega}},\boldsymbol{h}\rangle + |\tilde{\boldsymbol{\omega}}|\sqrt{\gamma(u)}y\right)$$
$$\times\, g(y)dy\frac{1}{(2\pi)^{k/2}}\exp\left(-\frac{|\tilde{\boldsymbol{\omega}}|^2}{2}\right)d\tilde{\boldsymbol{\omega}}\mu(dr)$$
$$= \frac{1}{(2\pi)^{k/2}}\int_{\mathbb{R}_+}\int_{\mathbb{R}^k}\cos\left(\sqrt{2r}\,\langle\tilde{\boldsymbol{\omega}},\boldsymbol{h}\rangle\right)$$
$$\times \int_{\mathbb{R}}\cos\left(|\tilde{\boldsymbol{\omega}}|\sqrt{\gamma(u)}y\right)g(y)dy\,\exp\left(-\frac{|\tilde{\boldsymbol{\omega}}|^2}{2}\right)d\tilde{\boldsymbol{\omega}}\mu(dr). \quad (31)$$

The last equality in (31) stems from the angle-sum trigonometric identity and the fact that $\langle\tilde{\boldsymbol{\omega}},\boldsymbol{h}\rangle$ is an odd function of $\tilde{\boldsymbol{\omega}}$ and $|\tilde{\boldsymbol{\omega}}|\sqrt{\gamma(u)}y$ is an even function of $\tilde{\boldsymbol{\omega}}$.

The simulated random field $Z$ is therefore second-order stationary, since its expectation is identically zero and the covariance between any two variables $Z(\boldsymbol{x},t)$ and $Z(\boldsymbol{x}',t')$ only depends on $\boldsymbol{h} = \boldsymbol{x}-\boldsymbol{x}'$ and $u = t-t'$. Up to a multiplicative factor, the last integral in (31) appears as the Fourier transform of the standard Gaussian probability density $g(y)$ on $\mathbb{R}$. Specifically:

$$\int_{\mathbb{R}}\cos\left(|\tilde{\boldsymbol{\omega}}|\sqrt{\gamma(u)}y\right)g(y)dy = \exp\left(-|\tilde{\boldsymbol{\omega}}|^2\frac{\gamma(u)}{2}\right).$$

Hence:

$$\mathbb{E}[Z(\boldsymbol{x},t)Z(\boldsymbol{x}',t')]$$
$$= \frac{1}{(2\pi)^{k/2}}\int_{\mathbb{R}_+}\int_{\mathbb{R}^k}\cos(\sqrt{2r}\,\langle\tilde{\boldsymbol{\omega}},\boldsymbol{h}\rangle)$$
$$\times\exp\left(-|\tilde{\boldsymbol{\omega}}|^2\frac{\gamma(u)+1}{2}\right)d\tilde{\boldsymbol{\omega}}\mu(dr)$$
$$= C(\boldsymbol{h},u). \quad (32)$$

The last equality in (32) stems from (11) and completes the proof. □

## References


Arroyo, D., Emery, X.: Simulation of intrinsic random fields of order $k$ with Gaussian generalized increments by Gibbs sampling. Math. Geosci. **47**(8), 955–974 (2015)

Barabesi, L., Pratelli, L.: Universal methods for generating random variables with a given characteristic function. J. Stat. Comput. Simul. **85–8**, 1679–1691 (2015)

Bernstein, S.: Sur les fonctions absolument monotones. Acta Math. **52**, 1–66 (1929)

Bochner, S.: Harmonic Analysis and the Theory of Probability. University of California Press, Berkeley (1955)

Bondesson, L.: On simulation from infinitely divisible distributions. Adv. Appl. Probab. **14**(4), 855–869 (1982)

Bourotte, M., Allard, D., Porcu, E.: A flexible class of non-separable cross-covariance functions for multivariate space-time data. Spat. Stat. **18**, 125–146 (2016)

Box, G., Muller, M.: A note on the generation of random normal deviates. Ann. Math. Stat. **29**(2), 610–611 (1958)

Brix, A.: Generalized gamma measures and shot-noise Cox processes. Adv. Appl. Probab. **31**(4), 929–953 (1999)

Carrizo-Vergara, R., Allard, D., Desassis, N.: A general framework for SPDE-based stationary random fields (2018). arXiv preprint arXiv:1806.04999

Chambers, J., Mallows, C., Stuck, B.: A method for simulating stable random variables. J. Am. Stat. Assoc. **71**(354), 340–344 (1976)

Chan, G., Wood, A.T.: Simulation of stationary Gaussian vector fields. Stat. Comput. **9**(4), 265–268 (1999)

Chilès, J.-P., Delfiner, P.: Geostatistics: Modeling Spatial Uncertainty, 2nd edn. Wiley, London (2012)

Cox, D.R., Isham, V.: A simple spatial-temporal model of rainfall. Proc. R. Soc. Lond. A Math. Phys. Sci. **415**(1849), 317–328 (1988)

Cuevas, F., Porcu, E., Bevilacqua, M.: Contours and dimple for the Gneiting class of space-time correlation functions. Biometrika **101**(4), 995–1001 (2017)

Davis, M.: Production of conditional simulations via the LU triangular decomposition of the covariance matrix. Math. Geol. **19**(2), 91–98 (1987)

De Iaco, S., Myers, D.E., Posa, D.: Space-time analysis using a general product-sum model. Stat. Probab. Lett. **52**(1), 21–28 (2001)
Devroye, L.: Non-Uniform Random Variate Generation. Springer, Berlin (1986)
Devroye, L.: The computer generation of random variables with a given characteristic function. Comput. Math. Appl. **7**, 547–552 (2001)
Devroye, L.: Random variate generation for exponentially and polynomially tilted stable distributions. ACM Trans. Model. Comput. Simul. **19–4**, 1–20 (2009)
Dietrich, C., Newsam, G.: Fast and exact simulation of stationary Gaussian processes through circulant embedding of the covariance matrix. SIAM J. Sci. Comput. **18**(4), 1088–1107 (1997)
Emery, X.: Statistical tests for validating geostatistical simulation algorithms. Comput. Geosci. **34**(11), 1610–1620 (2008a)
Emery, X.: Substitution random fields with Gaussian and gamma distributions: theory and application to a pollution data set. Math. Geosci. **40**(1), 83–99 (2008b)
Emery, X., Lantuéjoul, C.: Tbsim: a computer program for conditional simulation of three-dimensional Gaussian random fields via the turning bands method. Comput. Geosci. **32**(10), 1615–1628 (2006)
Feller, W.: An Introduction to Probability Theory and its Applications, vol. II. Wiley, London (1966)
Gneiting, T.: Nonseparable, stationary covariance functions for space-time data. J. Am. Stat. Assoc. **97**(458), 590–600 (2002)
Gneiting, T., Guttorp, P.: Continuous parameter spatio-temporal processes. Handb. Spat. Stat. **97**, 427–436 (2010)
Gneiting, T., Sasvári, Z., Schlather, M.: Analogies and correspondences between variograms and covariance functions. Adv. Appl. Probab. **33**(3), 617–630 (2001)
Gneiting, T., Schlather, M.: Stochastic models that separate fractal dimension and the Hurst effect. SIAM Rev. **46**(2), 269–282 (2004)
Kent, J.T., Mohammadzadeh, M., Mosammam, A.M.: The dimple in Gneiting's spatial-temporal covariance model. Biometrika **98**(2), 489–494 (2011)
Khintchine, A., Lévy, P.: Sur les lois stables. Compte Rendus de l'académie des Sciences de Paris **202**, 374–376 (1936)
Kolmogorov, A.: The local structure of turbulence in incompressible viscous fluid at very large Reynolds numbers. In: Friedlander, S., Topping, L. (eds.) Turbulence: Classic Papers on Statistical Theory, pp. 151–155. Interscience Publishers, New York (1961)
Lancaster, H.-O.: Some properties of the bivariate normal distribution considered in the form of a contingency table. Biometrika **44**(1–2), 289–292 (1957)
Lantuéjoul, C.: Ergodicity and integral range. J. Microsc. **161**(3), 387–404 (1991)
Lantuéjoul, C.: Non conditional simulation of stationary isotropic multigaussian random functions. In: Armstrong, M., Dowd, P.A. (eds.) Geostat. Simul., pp. 147–177. Kluwer Academic Publishers, Dordrecht (1994)
Lantuéjoul, C.: Geostatistical Simulation: Models and Algorithms. Springer, Berlin (2002)
Ma, C.: Spatio-temporal covariance functions generated by mixtures. Math. Geol. **34**(8), 965–975 (2002)
Ma, C.: Families of spatio-temporal stationary covariance models. J. Stat. Plan. Inference **116**(2), 489–501 (2003)
Matheron, G.: Leçon sur les fonctions aléatoires d'ordre 2. Technical report, Centre de Géostatistique, Ecole des Mines de Paris, C-53 (1972)
Matheron, G.: The intrinsic random functions and their applications. Adv. Appl. Probab. **4–3**, 508–541 (1973)
Matheron, G.: La déstructuration des hautes teneurs et le krigeage des indicatrices. Technical report, Centre de Géostatistique, École des Mines de Paris (1982)
Oberhettinger, F., Badii, L.: Tables of Laplace Transforms. Springer, New York (1973)
Sato, K.: Absolute continuity of multivariate distributions of class L. J. Multivar. Anal. **12**(1), 89–94 (1982)
Schilling, R., Song, R., Vondraček, Z.: Bernstein Functions. De Gruyter, Berlin (2010)
Schlather, M.: Some covariance models based on normal scale mixtures. Bernoulli **16**(3), 780–797 (2010)
Schlather, M.: Construction of covariance functions and unconditional simulation of random fields. In: Advances and Challenges in Space-Time Modelling of Natural Events, pp. 25–54. Springer (2012)
Schlather, M., Malinowski, A., Menck, P.J., Oesting, M., Strokorb, K., et al.: Analysis, simulation and prediction of multivariate random fields with package RandomFields. J. Stat. Softw. **63**(8), 1–25 (2015)
Schlather, M., Malinowski, A., Oesting, M., Boecker, D., Strokorb, K., Engelke, S., Martini, J., Ballani, F., Moreva, O., Auel, J., Menck, P.J., Gross, S., Ober, U., Ribeiro, P., Ripley, B.D., Singleton, R., Pfaff, B., R Core Team: RandomFields: Simulation and Analysis of Random Fields. R package version 3.3.8 (2020)
Schlather, M., Moreva, O.: A parametric model bridging between bounded and unbounded variograms. Stat **6**(1), 47–52 (2017)
Schoenberg, I.-J.: Metric spaces and completely monotone functions. Ann. Math. **39**(4), 811–831 (1938)
Shinozuka, M.: Simulation of multivariate and multidimensional random processes. J. Acoust. Soc. Am. **49**(1B), 357–367 (1971)
White, P., Porcu, E.: Towards a complete picture of stationary covariance functions on spheres cross time. Electr. J. Stat. **13**, 2566–2594 (2019)
Wood, A.T., Chan, G.: Simulation of stationary Gaussian processes in $[0, 1]^d$. J. Comput. Graph. Stat. **3**(4), 409–432 (1994)
Yaglom, A.: Some classes of random fields in $n$-dimensional space, related to stationary random processes. Theory Probab. Its Appl. **2–3**, 273–320 (1957)
Zastavnyi, V.P., Porcu, E.: Characterization theorems for the Gneiting class of space-time covariances. Bernoulli **17**(1), 456–465 (2011)